Inorg. Chem. **2008**, *47*, 10816−10824

Probing the Electronic Communication of the Isocyanide Bridge Through the Luminescence Properties of the d^9-d^9 $[ClPt(\mu\text{-dppm})_2Pt(C{\equiv}N{-}PCP)]^+$ and A-Frame $[ClPd(\mu\text{-dppm})_2(\mu\text{-}C{=}N{-}PCP)PdCl]$ Complexes

Sébastien Clément,[†] Shawkat Mohammed Aly,[†] Daniel Fortin,[†] Laurent Guyard,[‡] Michael Knorr,*[,‡] Alaa S. Abd-El-Aziz,[§] and Pierre D. Harvey*[,†]

Département de chimie, Université de Sherbrooke, 2550 Boul. Université, Sherbrooke, PQ, Canada, J1K 2R1, the Institut UTINAM UMR CNRS 6213, Université de Franche-Comté, Faculté des Sciences et des Techniques, La Bouloie - 16 Route de Gray, F-25030 Besançon, France, Department of Chemistry, and the University of British Columbia Okanagan, 3333 University Way, Kelowna, BC, Canada, V1V 1V7

Received May 5, 2008

The homodinuclear d^9-d^9 $ClM(\mu\text{-dppm})_2MCl_2$ complexes, **1** (M = Pt) and **2** (M = Pd) react with the conjugated and luminescent PCP−NC ligand (**3**, PCP = [2.2]paracyclophane) to provide the corresponding d^9-d^9 terminal $[ClPt(\mu\text{-dppm})_2Pt(CN{-}PCP)]Cl$ (**4**) and d^8-d^8 A-frame $[ClPd(\mu\text{-dppm})_2(\mu\text{-}C{=}N{-}PCP)PdCl]$ (**5**) isocyanide complexes, respectively. These two bimetallic complexes were characterized by IR, ^1H, and $^{31}P\{^1H\}$ NMR and by chemical analysis. IR data (ν(CN) bridging vs terminal) reveal a terminal isocyanide bonding mode for **4** (2147 cm^{-1}) and an A-frame structure for **5** (1616 cm^{-1}). The optical and emission properties of the free isocyanide **3** as well as those of the homodinuclear complexes **4** and **5** were studied by UV−visible and luminescence spectroscopy and by photophysical measurements. The unexpected presence of simultaneous intraligand $\pi\pi^*$ fluorescence and phosphorescence attributable to the organic PCP−NC ligand, as well as luminescence from the inorganic M_2-bonded $Pt_2(\mu\text{-dppm})_2$ center arising from a lower energy excited LMCT state (ligand-to-metal-charge-transfer) for **4** at 77 K, indicates a weak conjugation between the two chromophores and an absence of efficient singlet and triplet energy transfers. For **5**, only the fluorescence and phosphorescence bands of the PCP−NC ligand are observed [since the A-frame $XPd(\mu\text{-dppm})_2(\mu\text{-L})PdX$ (L = isocyanide, X = halide) is not luminescent], stressing that the N≡C bridge exhibits modest electronic communication properties.

Introduction

[2.2]Paracyclophanes (PCP) constitute an intriguing class of compounds that have attracted the interest of many researchers since the synthesis of the parent compound around the middle of this century.[1] Numerous PCP derivatives were prepared for various applications such as chiral catalysis,[2] the design of new nonlinear optical (NLO) materials,[3] π-conjugated arrays, electron transfer processes, and molecular electronics.[4] The unique structural and electronic properties of these derivatives arise from the characteristic interactions between the two cofacial π-electron systems.[5,6]

We reported the physicochemical properties of oligomeric and polymeric dppm-spanned Pd−Pd and Pt−Pt arrays assembled by unconjugated and conjugated diisocyanide

* To whom correspondence should be addressed. Phone: [33] 3 81 66 62 70 (M.K.), (819) 821-7092 (P.D.H.); fax: +[33] 3 81 66 64 38 (M.K.), (819) 821-8017 (P.D.H.); e-mail: michael.knorr@univ-fcomte.fr (M.K.), Pierre.Harvey@USherbrooke.ca (P.D.H.).

[†] Université de Sherbrooke.

[‡] Université de Franche-Comté.

[§] University of British Columbia Okanagan.

(1) Brown, C. J.; Farthing, A. C. *Nature* **1949**, *164*, 915–916.

(2) (a) Bräse, S.; Dahmen, S. *Chem. Commun.* **2002**, 26–27. (b) Kreis, M.; Nieger, M.; Bräse, S. *J. Organomet. Chem.* **2006**, *691*, 2171–2181. (c) Pye, P. J.; Rossen, K.; Reamer, R. A.; Volante, R. P.; Reider, P. J. *Tetrahed. Lett.* **1998**, *39*, 4441–4444.

(3) (a) Verdal, N.; Godbout, J. T.; Perkins, T. L.; Bartholomew, G. P.; Bazan, G. C.; Kelly, A. M. *Chem. Phys. Lett.* **2000**, *320*, 95–103. (b) Bartholomew, G. P.; Bazan, G. C. *J. Am. Chem. Soc.* **2002**, *124*, 5183–5196. (c) Popova, E. L.; Rozenberg, V. I.; Starikova, A.; Keuker-Baumann, S.; Kitzerow, H. S.; Hopf, H. *Angew. Chem. Ind. Ed.* **2002**, *41*, 3411–3414. (d) Amthor, S.; Lambert, C.; Dümmler, S.; Fischer, I.; Schelter, J. *J. Phys. Chem. A* **2006**, *110*, 5204–5214.

10.1021/ic800811j CCC: $40.75
Published on Web 10/25/2008

Chart 1

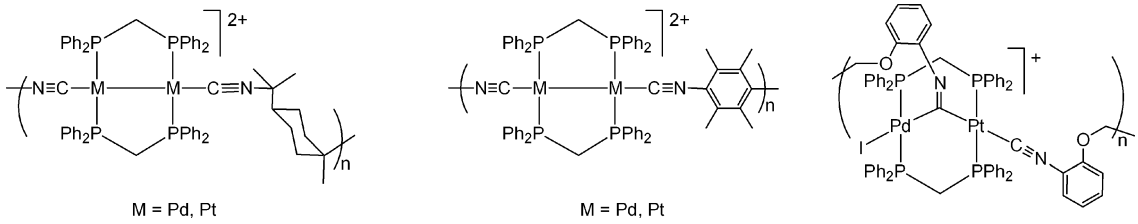

Chart 2

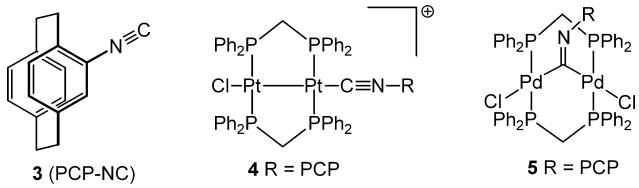

ligands (Chart 1).[7,8] The unconjugated polymers were those using the saturated dmb ligand (1,8-diisocyano-*p*-menthane), and the conjugated ones were built upon *para*-diisocyanotetramethylbenzene. The conjugation was demonstrated by the red-shift of the absorption bands going from the monomeric models [M(μ-dppm)$_2$(μ-C═N−C$_6$H$_4$−*i*Pr)$_2$M]$^{2+}$ (M = Pd, Pt) to the polymers and by the increased thermal stability in the polymers by comparison with the same models. We also recently reported the first A-frame-containing organometallic/coordination polymer arising from the reaction between the corresponding d^9−d^9 MM′-bonded complex (M = Pd, M′ = Pt) and the 1,2-bis-(2-isocyanophenoxy)ethane assembling ligand. The material is found to be strongly luminescent at 77K.[9]

We now wish to report the chemical and photophysical properties of homodinuclear Pd−Pd and Pt−Pt complexes containing PCP−NC (Chart 2). The PCP−NC ligand was chosen because the PCP-containing compounds exhibit luminescence. It is demonstrated that the use of a heavy metal (here as Pd$_2$- or Pt$_2$(μ-dppm)$_2$) promotes intersystem crossing, hence populating the triplet excited-state of the organic component (here [2.2]paracyclophane), but also proportionally depopulating the singlet excited state. In addition, this paper shows that electronic communication between the PCP lumophore and both the [ClPt(μ-dppm)$_2$Pt(CN−R)]$^+$ and [ClPd(μ-dppm)$_2$(μ-C═N−R)PdCl] units is relatively modest despite conjugation.

Experimental Section

Materials. All reactions were performed in Schlenk-tubes under purified nitrogen. Compounds ClPd(μ-dppm)$_2$PdCl (**1**), ClPt-(μ-dppm)$_2$PtCl (**2**), and PCP−NC (**3**) were prepared according to literature methods.[10−12] All solvents were dried and distilled from appropriate drying agents.

[ClPt(μ-dppm)$_2$Pt(CNPCP)]Cl (4). Compound **3** (0.023 g, 0.100 mmol) was dissolved in 2 mL of CH_2Cl_2 and was added over a period of 30 min to a stirred solution of **2** (0.123 g, 0.1 mmol) in 3 mL of CH_2Cl_2. The yellowish solution was stirred for 1 h and evaporated to dryness. The yellow residue was washed with 3 mL of Et_2O and dried under vacuum. Yield: 0.133 g (91%). IR (CH_2Cl_2): 2147(s) cm^{-1} (ν_{CN}); ^{1}H NMR ($CDCl_3$): δ 8.59−6.26 (m, 47 H, Ph), 4.61 (m, br, 4 H, PC*H*$_2$P), 3.15−2.47 (m, 8 H, C*H*$_2$). ^{31}P{^{1}H} NMR ($CDCl_3$): δ 7.3 (m, 2 P, $^1J_{Pt-P}$ = 2020), 2.7 (m, 2 P, $^1J_{Pt-P}$ = 2925) ppm. Anal. calcd for $C_{67}H_{59}Cl_2NP_4Pt_2\cdot CH_2Cl_2$: C, 52.71; H, 3.94; N, 1.05. Found C, 52.66; H, 3.83; N, 1.00. The presence of CH_2Cl_2 was confirmed by ^{1}H NMR.

[ClPd(μ-dppm)$_2$(μ-C═N−PCP)PdCl] (5). Compound **3** (0.023 g, 0.100 mmol) was dissolved in 2 mL of CH_2Cl_2 and was added over a period of 30 min to a stirred solution of **1** (0.105 g, 0.100 mmol) in 3 mL of CH_2Cl_2. The reddish solution was stirred for 1 h and evaporated to dryness. The red residue was washed with 3 mL of Et_2O and dried under vacuum. Yield: 0.118 g (92%). IR (KBr): 1616(w) ($\nu_{C=N}$) cm^{-1}. ^{1}H NMR ($CDCl_3$): δ 7.01−8.30 (m, 40 H, Ph), 6.36 (s, 1 H), 6.33 (d, 1 H$_{aromatic}$, $^3J_{H-H}$ = 7.9), 6.28 (d, 1 H$_{aromatic}$, $^3J_{H-H}$ = 7.9), 6.09 (d, 1 H$_{aromatic}$, $^3J_{H-H}$ = 7.9), 6.01 (d, 1 H$_{aromatic}$, $^3J_{H-H}$ = 7.9), 5.70 (d, 1 H$_{aromatic}$, $^3J_{H-H}$ = 7.9), 5.62 (d, 1 H$_{aromatic}$, $^3J_{H-H}$ = 7.9), 2.79 (m, 4 H, PC*H*$_2$P), 2.10−2.52 (m, 8 H, C*H*$_2$), ppm. ^{31}P{^{1}H} NMR ($CDCl_3$): δ 17.4 (m, 4P, br.) ppm. Anal. calcd for $C_{67}H_{59}Cl_2NP_4Pd_2\cdot 0.5CH_2Cl_2$: C, 60.97; H, 4.52; N, 1.05. Found: C, 60.87; H, 4.48; N, 0.98. The presence of CH_2Cl_2 was confirmed by ^{1}H NMR.

Apparatus. IR spectra have been recorded on a Nicolet Nexus 470 spectrometer. All NMR spectra were acquired with a Bruker Avance 300 (^{1}H 300.13 MHz, ^{13}C 75.48 MHz, and ^{31}P 121.49 MHz) using the solvent as the chemical shift standard, except for ^{31}P NMR, where the chemical shifts are relative to H_3PO_4 85% in D_2O. All the chemical shifts and coupling constants are reported in ppm and Hz, respectively. UV−vis spectra were recorded on a Varian Cary 50 spectrophotometer. Emission and excitation spectra were obtained using a double monochromator Fluorolog 2 instrument

(4) (a) Aly, A. A.; Ehrhardt, S.; Hopf, H.; Dix, I.; Jones, P. G. *Eur. J. Org. Chem.* **2006**, 335–350. (b) Hu, W.; Gompf, B.; Pflaum, J.; Schweitzer, D.; Dressel, M. *Appl. Phys. Lett.* **2004**, *84*, 4720–4722. (c) Hopf, H.; Sankararaman, S.; Dix, I.; Jones, P. G.; Alt, H. G.; Licht, A. *Eur. J. Inorg. Chem.* **2002**, 123–131. (d) Lahann, J.; Höcker, H.; Langer, R. *Angew. Chem., Int. Ed. Engl.* **2001**, *40*, 726–728.

(5) (a) Hopf, H.; Gleiter, R. *Modern Cyclophane Chemistry*; Wiley-VCH: Weinheim, 2004. (b) De Meijere, A.; König, B. *Synlett.* **1997**, 1221–1232.

(6) (a) Ball, P. J.; Shtoyko, T. R.; Bauer, J. A. K.; Oldham, W. J.; Connick, W. B. *Inorg. Chem.* **2004**, *43*, 622–632. (b) Laganis, E. D.; Voegeli, R. H.; Swann, R. T.; Finke, R. G.; Hopf, H.; Boekelheide, V. *Organometallics* **1982**, 1415–1420. (c) Kang, H. C.; Plitzko, K.-D.; Boekelheide, V.; Higuchi, H.; Mitsumi, S. *J. Organomet. Chem.* **1987**, *321*, 79–89.

(7) Bérubé, J.-F.; Gagnon, K.; Fortin, D.; Decken, A.; Harvey, P. D. *Inorg. Chem.* **2006**, *45*, 2812–2823.

(8) (a) Harvey, P. D., *Frontiers in Transition Metal-Containing Polymers*; Wiley Interscience, John Wiley and Sons Inc.: New York, 2007; pp 321−368; (b) Harvey, P. D. In *Inorganic and Organometallic Macromolecules: Design and Applications*; Springer Science: New York, 2008; pp 71−108.

(9) Clément, S.; Mohammed Aly, S.; Gagnon, K.; Abd-El-Aziz, A. S.; Knorr, M.; Harvey, P. D. *J. Inorg. Organomet. Polym.* **2008**, *18*, 104–110.

(10) Clément, S.; Guyard, L.; Knorr, M.; Dilsky, S.; Strohmann, C.; Arroyo, M. *J. Organomet. Chem.* **2007**, *692*, 839–850.

(11) Grossel, M. C.; Batson, J. R.; Moulding, R. P.; Seddon, K. R. *J. Organomet. Chem.* **1986**, *304*, 391–423.

(12) Pringle, P. G.; Shaw, B. L. *J. Chem. Soc., Dalton Trans.* **1983**, 889–897.

Scheme 1

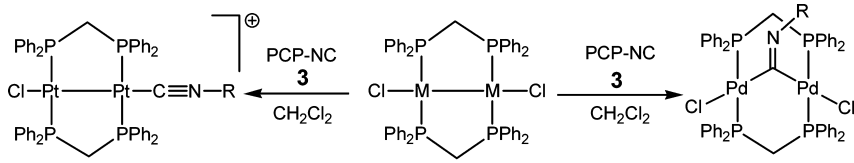

4 R = PCP

1 M = Pd
2 M = Pt

5 R = PCP

from Spex. Fluorescence lifetimes were measured on a Timemaster model TM-3/2003 apparatus from PTI. The source was a nitrogen laser equipped with a high-resolution dye laser (fwhm ≈ 1500 ps), and the fluorescence lifetimes were obtained from deconvolution and distribution lifetime analysis. The quantum yield was measured against $[Ru(bpy)_3](Cl)_2$ ($\Phi_e = 0.376 \pm 0.036$) in PrCN.[13]

Computations. All calculations were performed on an Pentium 3.20 GHz PC with the Gaussian 03 revision C.02 and Gausview 3.0 software package.[14] The hybrid B3LYP exchange−correlation function has been considered due to the high accuracy of the ensued results.[15−17] LANL2DZ[18−20] pseudopotentials were used on platinum, and 3−21G*[21] was used on phosphorus and chloride atoms, with LANL2DZ basis set for platinum and 3−21G* on phosphorus and chloride atoms. 6−31G[22,23] basis sets were used on all other atoms. The complexes were optimized to their ground singlet and triplet states, respectively, to calculate the HSOMO and HOMO energy difference to evaluate the phosphorescence wavelength.[24] The singlet ground state (S_0) was used to calculated the 0−0 TDDFT[25] $S_0 \cdots S_1$ absorption energy and oscillator strengths. The methodology was calibrated against the optimized geometry of the related X-ray characterized $[Pt_2(\mu\text{-dppm})_2(CN-t\text{Bu})_2]^{2+}$ cation (Supporting Information), and selected computed bond distances and angles for the optimized **3**, **4**, and **5** can be found in the Supporting Information.

Results and Discussion

Syntheses and Characterization. The homodinuclear complexes **4** and **5** are prepared from the reaction between the d^9-d^9 precursors $ClPd(\mu\text{-dppm})_2PdCl$ (**1**) or $ClPt(\mu\text{-dppm})_2PtCl$ (**2**) and the PCP-NC ligand (**3**) in a 1:1 complex-to-ligand ratio (Scheme 1).

The reaction product is governed by the nature of M. Indeed, whereas treatment of **2** with PCP−NC (**3**) produces exclusively the d^9-d^9 Pt−Pt-bonded monocationic species $[ClPt(\mu\text{-dppm})_2Pt(CN-PCP)]Cl$ (**4**) bearing a terminal CNR ligand, reaction of **1** with **3** under similar conditions leads to the d^8-d^8 A-frame compound $[ClPd(\mu\text{-dppm})_2(\mu\text{-C}=\text{N}-PCP)PdCl]$ (**5**), resulting from insertion of **3** into the Pd−Pd bond. The bridging or terminal bonding mode of the isocyanide ligand is deduced from the IR spectrum, which displays a $\nu(C=N)$ medium intensity peak at 1616 cm^{-1} for **5** and a strong $\nu(C\equiv N)$ band at 2147 cm^{-1} for **4**. The $^{31}P\{^1H\}$ NMR spectrum of **5** exhibits a very broad singlet-like resonance at $\delta = 17.4$ ppm. The broadness of this peak can be rationalized by fluxionality of the complex, leading to equilibration of **4** either by a "windscreen-wiper" motion of the bent C=N−PCP ligand in solution, leading to the quasiequivalence of the four phosphorus nuclei[26] or by an accidental near equivalence of the two P_A and P_B resonances.[27] Due to dissymmetry of **4**, its $^{31}P\{^1H\}$ NMR spectrum gives rise to a pattern characteristic of a AA′BB′ spin system consisting of two slightly broadened multiplets centered at 7.3 and 2.7 ppm with $^1J_{Pt-P}$ couplings of 2020 and 2925 Hz, respectively.

Photophysical Properties. The absorption spectrum of phane was previously studied in great detail.[5a,28,29] The close proximity of the two benzene rings (3.1 Å) gives rise to abnormal absorption bands that cannot be traced back to the usual $\pi\pi^*$ signature of benzene. It exhibits intense, short wavelength absorptions around 300 nm. These bands are

(13) Demas, J. N.; Crosby, G. A. *J. Am. Chem. Soc.* **1971**, *93*, 2841–2847.
(14) Frisch, M. J.; Trucks, G. W.; Schlegel, H. B.; Scuseria, G. E.; Robb, M. A.; Cheeseman, J. R.; Montgomery, J. A.; Vreven, J. T.; Kudin, K. N., Burant, J. C.; Millam, J. M.; Iyengar, S. S.; Tomasi, J.; Barone, V.; Mennucci, B., Cossi, M., Scalmani, G.; Rega, N.; Petersson, G. A.; Nakatsuji, H.; Hada, M.; Ehara, M.; Toyota, K.; Fukuda, R.; Hasegawa, J.; Ishida, M.; Nakajima, T.; Honda, Y.; Kitao, O. Nakai, H Klene, M. Li, X. Knox, J. E. Hratchian, H. P.; Cross, J. B. Adamo, C. Jaramillo, J. Gomperts, R. Stratmann, R. E. Yazyev, O. Austin, A. J. Cammi, R. Pomelli, C. Ochterski, J. W. Ayala, P. Y. Morokuma, K. Voth, G. A. Salvador, P. Dannenberg, J. J. Zakrzewski, V. G. Dapprich, S. Daniels, A. D. Strain, M. C. Farkas, O. Malick, D. K. Rabuck, A. D. Raghavachari, K. Foresman, J. B. Ortiz, J. V. Cui, Q. Baboul, A. G. Clifford, S. Cioslowski, J. Stefanov, B. B. Liu, G. Liashenko, A. Piskorz, P. Komaromi, I. Martin, R. L. Fox, D. J. Keith, T. Al-Laham, M. A. Peng, C. Y. Nanayakkara, A. Challacombe, M. Gill, P. M. W. Johnson, B. Chen, W. Wong, M. W. Gonzalez, C. Pople, J. A. *Gaussian 03, Revision C.02*; Gaussian,Inc.: Wallingford CT, 2004.
(15) Becke, A. D. *J. Chem. Phys.* **1993**, *98*, 5648–5652.
(16) Lee, C.; Yang, W.; Parr, R. G. *Phys. Rev. B: Condens. Matter Mater. Phys.* **1988**, 785–789.
(17) Miehlich, B.; Savin, A.; Stoll, H.; Preuss, H. *Chem. Phys. Lett.* **1989**, *157*, 200–206.
(18) Hay, P. J.; Wadt, W. R. *J. Chem. Phys.* **1985**, *82*, 270–283.
(19) Wadt, W. R.; Hay, P. J. *J. Chem. Phys.* **1985**, *82*, 284–298.
(20) Hay, P. J.; Wadt, W. R. *J. Chem. Phys.* **1985**, *82*, 299–310.
(21) Dobbs, K. D.; Hehre, W. J. *J. Comput. Chem.* **1987**, *8*, 880–893.
(22) Ditchfield, R.; Hehre, W. J.; Pople, J. A. *J. Chem. Phys.* **1971**, *54*, 724–728.
(23) Hehre, W. J.; Ditchfield, R.; Pople, J. A. *J. Chem. Phys.* **1972**, *56*, 2257–2261.
(24) Lowry, M. S.; Hudson, W. R.; Pascal, R. A., Jr.; Bernhard, S. *J. Am. Chem. Soc.* **2004**, *43*, 14129–14135.
(25) (a) Stratmann, R. E.; Scuseria, G. E.; Frisch, M. J. *J. Chem. Phys.* **1998**, *109*, 8218. (aa) Bauernschmitt, R.; Ahlrichs, R. *Chem. Phys. Lett.* **1996**, *256*, 454. (b) Casida, M. E.; Jamorski, C.; Casida, K. C.; Salahub, D. R. *J. Chem. Phys.* **1998**, *108*, 4439.
(26) (a) Evrard, D.; Clément, S.; Lucas, D.; Hanquet, B.; Knorr, M.; Strohmann, C.; Decken, A.; Mugnier, Y.; Harvey, P. D. *Inorg. Chem.* **2006**, *45*, 1305–1315. (b) We have recently prepared the A-frame complex $[ClPd(\mu\text{-dppm})_2(\mu\text{-C}=\text{N}-C_6H_4Pr^i)PdCl]$, whose four ^{31}P nuclei give rise to a sharp singlet at δ 17.8, proofing the fluxionality of this type of compounds.
(27) An AA′BB′ pattern was observed for the $^{31}P\{^1H\}$ NMR spectrum of $[ClPd(\mu\text{-dppm})_2(\mu\text{-N}=\text{N}-C_6H_4OCH_3)PdCl]BF_4$. See: Neve, F.; Longeri, M.; Ghedini, M.; Crispini, A. *Inorg. Chim. Acta* **1993**, *205*, 15–22.
(28) (a) Bazan, G. C.; Jr, W. J. O.; Lachicotte, R. J.; Tretiak, S.; Chernyak, V.; Mukamel, S. *J. Am. Chem. Soc.* **1998**, *120*, 9188–9204. (b) Bartholomew, G. P.; Bazan, G. C. *Acc. Chem. Res.* **2001**, *34*, 30–39.
(29) (a) Cram, D. J.; Allinger, N. L.; Steinberg, H. *J. Am. Chem. Soc.* **1954**, *76*, 6132–6141. (b) Iwata, S.; Fuke, K.; Sasaki, M.; Nagakura, S.; Otsubo, T.; Misumi, S. *J. Mol. Spectrosc.* **1973**, *46*, 1–15. (c) Hillier, I. H.; Rice, S. A. *J. Chem. Phys.* **1966**, *45*, 4639–4642. (d) Froines, J. R.; Hagerman, P. J. *Chem. Phys. Lett.* **1969**, *4*, 135–138. (e) Canuto, S.; Zerner, M. C. *J. Am. Chem. Soc.* **1990**, *112*, 2114–2120.

Table 1. Absorption Data for Compounds **3**−**5** in 2-MeTHF at 298 K

compound	λ_{max} (ε, $M^{-1}\cdot cm^{-1}$)
3	268 (21 000), 294 (6300), 322 (1800)
4	273 (16 200), 314 (6300), 364 (3600), 415 (1100)
5	286 (17 800), 445 (2500)

assigned to the π-electron system, which is modified by the loss of planarity and the strong transannular interactions of both benzene rings, whereas the band around 320 nm (respectively, $\varepsilon = 1800\ M^{-1}\cdot cm^{-1}$ in 2-MeTHF and $\varepsilon = 1900\ M^{-1}\cdot cm^{-1}$ in PrCN) can in first instance be tentatively assigned to the $\pi\pi^*$ transition of the conjugated isocyanide-containing benzene ring (Table 1).

At 77 K in frozen PrCN and 2-MeTHF, the coordinated PCP−NC ligand exhibits two broad (full-width-at-half-maximum, fwhm = 12 000 and 45 000 cm^{-1}, respectively) unstructured emissions at λ_{max} around 370 and 480 nm, typical for excimers and phanes (Figure 1 and Supporting Information). The emission maxima are not shifted using different solvents. This absence of a solvatochromatic effect is consistent with a similar charge distribution of the ground-state and the emitting state. The first emission maximum is assigned to fluorescence (fluorescence lifetime, $\tau_F \approx 1.23$ ns in 2-MeTHF and $\tau_F \approx 1.85$ ns in PrCN) (Table 2). The τ_F values using PrCN and 2-MeTHF ($\tau \approx 1$ ns) compare very favorably with other π-conjugated systems incorporating the PCP skeleton, as previously described by Bazan et al.[28,30]

The second band is phosphorescence as deduced from the long lifetime ($\tau_P \approx 3.75$ s in 2-MeTHF, $\tau_P \approx 3.37$ s in PrCN). The time-resolved emission spectrum for **3** in PrCN at 77 K (see the Supporting Information) decays in the long time scale, and no other emission was detected, hence supporting this assignment. The wavelength maxima, emission lifetimes, and quantum yields compare favorably to that of other 4-substituted PCP derivatives.[31,32] The electronic spectra of **3** are very similar to other reported PCP derivatives, indicating only a moderate influence of the isocyanide group. The photophysical data for **3** are presented in Table 2. Compound **3** is also weakly luminescent at room temperature in solution (Figure 1b and Table 2) and in the solid state at 77K (Supporting Information, Table 2). The excitation spectrum superposes the absorption spectrum. No phosphorescence is observed at room temperature.

Figure 2 shows the HOMO − 1, HOMO, and LUMO for ligand **3** (optimized geometry). The lowest energy electronic transitions (HOMO − 1 → LUMO and HOMO → LUMO) are $\pi\pi^*$-type. The LUMO is composed mainly of p_x orbitals localized on the benzene ring bearing the CN group, whereas the HOMO is composed mostly of p_x orbitals centered on the benzene that has no substituent. The HOMO − 1 is also composed of p_x orbitals, but distributed over the two benzene rings. All in all, the two predicted lowest energy transitions are expected to exhibit some charge transfer (CT) character due to the symmetry of this ligand. Moreover, because of the poor orbital overlap between the HOMO and LUMO, the oscillator strength and the absorptivity are expected to be low. Indeed, experimentally the absorptivity values are 6300 for 294 nm absorption and 1800 $M^{-1}\cdot cm^{-1}$ for the 322 nm band. The lowest energy transitions (excited states 1, 2, and 3) are computed by TDDFT to be localized at 267, 281, and 296 nm (Table 3), respectively, which are in reasonable agreement with the experimental data presented in Table 1 (i.e., 268 (21 000), 294 (6300), and 322 nm (1800 $M^{-1}\cdot cm^{-1}$)). The red-shifted discrepancy is due to the fact that the calculated data are for gas phase molecules, whereas the experimental data for the ligand are obtained for 2-MeTHF as the solvent at 298 K. The fact that these excited states exhibit a CT character makes the sensitivity to solvent polarity more pronounced. The relative calculated oscillator strengths agree with the observed relative absorptivity data.

These calculated lowest energy transitions are composed of more than one transition. For excited state 1, the major component is expected to be mainly the HOMO → LUMO transition (62 → 63). Minor contributions arising from the HOMO − 1 → LUMO and HOMO → LUMO + 1 transitions are also computed. The other excited states are also composed of other transitions, and their nature appears more complex due to the higher number of contributions and the closeness of the relative probability of these components. So, the nature of the fluorescent state is a $\pi\pi^*$-system that exhibits a strong charge transfer character from the unsubstituted benzene ring to the NC-substituted one.

The nature of the phosphorescence is analyzed using DFT calculations of the optimized geometry of the ligand **3** in the triplet state. The calculated highest semioccupied MO (HSOMO) exhibits a similar atomic contribution of the LUMO of the diamagnetic S_0 molecule, except that the contribution of the p_x orbital of the unsubstituted ring has diminished significantly to −0.131 au. Upon relaxation via emission of a photon (i.e., phosphorescence), the triplet state geometry remains the same. So, the computed HOMO in its triplet geometry is also computed. It exhibits a modified atomic contribution scheme with respect to the HOMO in its ground state (S_0). Its MO energy is −0.212 au (higher than the HOMO in the ground state; −0.225 au). It is composed of the p_x orbitals of the substituted benzene ring including the NC group. This MO bears resemblance with the HSOMO rather than with the HOMO. The nuclear relaxation between the HOMO computed with geometries in the triplet and ground-state involves an 0.013 au energy difference, corresponding to 2850 cm^{-1} or 0.35 eV. The energy difference between the two MOs (HSOMO and HOMO) computed in the triplet state geometry is 0.081 au giving a calculated phosphorescence wavelength of 562 nm. Figure 2 summarizes the calculated energetics of the frontier MOs, explaining the lowest-energy absorption and phosphorescence of **3**. It is noteworthy that the electronic density travels across the two benzene rings going from the ground-

(30) (a) Hong, J. W.; Woo, H. Y.; Bazan, G. C. *J. Am. Chem. Soc.* **2005**, *127*, 7435–7443. (b) Masunov, A.; Tretiak, S.; Hong, J. W.; Liu, B.; Bazan, G. C. *J. Chem. Phys.* **2005**, *122*−10.

(31) (a) Hopf, H.; Haase, M.; Hunger, J.; Tochtermann, W.; Zander, M. *Chem. Phys. Lett.* **1986**, *127*, 145–148. (b) Hopf, H.; Laue, T.; Zander, M. Z. *Naturforsch* **1991**, *46a*, 815–818. (c) Hopf, H.; Zander, M.; Hermann, E. Z. *Naturforsch* **1987**, *42a*, 1041–1042.

(32) (a) Melzer, G.; Schweitzer, D.; Hausser, K. H.; Colpa, J. P.; Haenel, M. W. *Chem. Phys.* **1979**, *39*, 229–235. (b) Vala, M. T. J.; Hillier, I. H.; Rice, S. A.; Jortner, J. *J. Chem. Phys.* **1966**, *44*, 23–35.

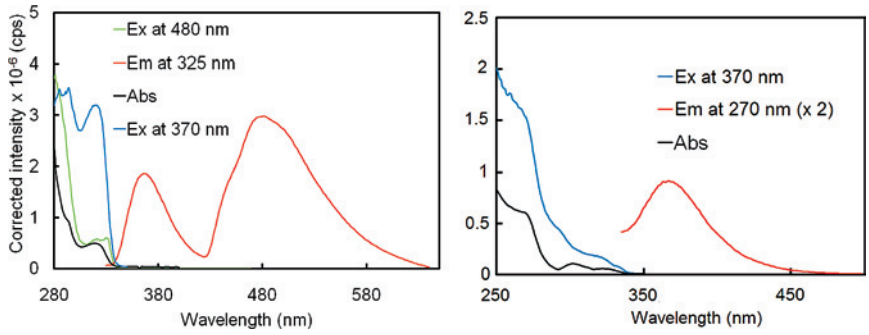

Figure 1. Absorption, excitation and emission spectra of **3** in PrCN at 77 K (left) and at 298 K (right).

Table 2. Photophysical Data for Compound **3**

	2-MeTHF (77 K)	PrCN (77 K)	PrCN (298 K)	solid (77 K)
λ_{abs} (nm)	274, 296, 310, 320 (sh)	295 (sh), 325	270, 302, 324 (sh)	[b]
λ_F (nm)	370	370	370	370
τ_F (ns)	1.23 ± 0.03	1.85 ± 0.22	0.63 ± 0.01	[b]
ϕ_F	[b]	0.089	0.02	
λ_P (nm)	480	480	[a]	500
τ_P (s)	3.75 ± 0.10	3.37 ± 0.18	[a]	[b]
ϕ_P[c]	[b]	0.048	[a]	

[a] No phosphorescence is observed at room temperature. [b] Not measured. [c] Measured against $[Ru(bpy)_3](Cl)_2$ (ϕ_e = 0.376 ± 0.036 in PrCN).[13]

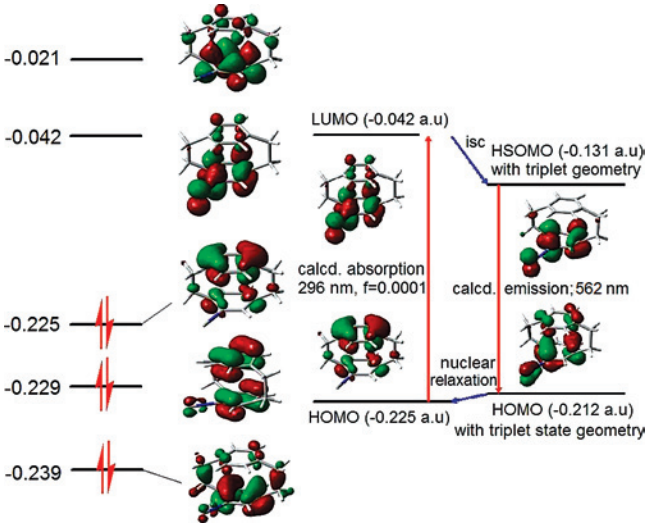

Figure 2. MO representation of the frontier MOs (left) and calculated energetics of the frontier orbitals explaining the lowest-energy absorption and phosphorescence of ligand **3**. The energy units are in a.u (right).

state, through the S_1 and T_1 levels, and then back to the ground state (Figure 2).

The UV−visible spectra of **4** exhibit bands below 320 nm, appearing as shoulders (Figure 3). A low-energy band (λ_{max} = 370 nm) is also observed and is associated with the Pt_2-containing fragment. At first glance, this band may be a typical $d\sigma \rightarrow d\sigma^*$ transition commonly known for d^9-d^9 M_2-bonded species.[33] However, the absorptivity data are a little small for such an assignment (ε = 3600 $M^{-1}\cdot cm^{-1}$ in 2-MeTHF and ε = 3400 $M^{-1}\cdot cm^{-1}$ in PrCN at 298 K, Table 1) in comparison with most absorptivity data for d^9-d^9 M_2-bonded species (ε > 10 000 $M^{-1}\cdot cm^{-1}$).[33] Figure 4 exhibits the frontier MOs going from HOMO − 5 to LUMO + 2 of the model complex $[Pt_2(PH_2CH_2PH_2)_2(Cl)(CNPCP)]^+$ (DFT). Both HOMOs are composed of π orbitals primarily located

Table 3. Computed Singlet−Singlet Transition Energies, Oscillator Strengths, and Their Components for **3**[a]

computed excited states and components (No. MO)		transition energies		oscillator strength
excited state 1:	62 → 63−0.65752	4.1950 eV	295.55 nm	f = 0.0001
	61 → 64 0.14959			
	61 → 63 0.14972			
excited state 2:	60 → 63 0.39749	4.4103 eV	281.13 nm	f = 0.0045
	61 → 63 0.47634			
	61 → 64−0.19240			
	62 → 63 0.16400			
	62 → 64−0.15866			
excited state 3:	60 → 63−0.38853	4.6508 eV	266.58 nm	f = 0.0312
	61 → 64 0.43853			
	61 → 64 0.27568			

[a] Transitions with f = 0 or 0.0001 are removed. MO 62 = HOMO; MO 63 = LUMO. The excited-state numbering refers to the order from the lowest energy to the highest. The positive and negative numbers beside the transition represent the relative probability (i.e., weighing).

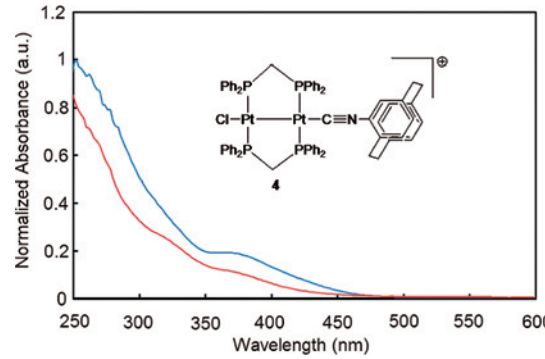

Figure 3. Absorption spectra of **4** in PrCN (red) and in 2-MeTHF (blue) at 298 K.

on the PCP residue. The HOMO (−0.309) is composed of occupied π orbitals located at the unfunctionalized ring of the PCP unit (where there is no CN group), whereas the π orbitals of HOMO − 1 (−0.316 au) are located on both rings of the PCP residue with practically no other atomic contribution. The LUMO is composed of d_z^2orbital forming the M_2 antibonding orbital plus some p_z component of the Cl atom and some p orbital of the CN unit. The LUMO + 1 is also composed of the same orbitals as for the LUMO but some minor contributions of the π system of the lower benzene ring is computed as well.

(33) (a) Sicard, S.; Bérubé, J.-F.; Samar, D.; Massaoudi, A.; Lebrun, F.; Fortin, J.-F.; Fortin, D.; Harvey, P. D. *Inorg. Chem.* **2004**, *43*, 5321–5334. (b) Fournier, E.; Sicard, S.; Decken, A.; Harvey, P. D. *Inorg. Chem.* **2004**, *43*, 1491–1501. (c) Zhang, T.; Drouin, M.; Harvey, P. D. *Inorg. Chem.* **1999**, *38*, 1305–1315. (d) Zhang, T.; Drouin, M.; Harvey, P. D. *Inorg. Chem.* **1999**, *38*, 957–963. (e) Harvey, P. D.; Murtaza, Z. *Inorg. Chem.* **1993**, *32*, 4721–4729.

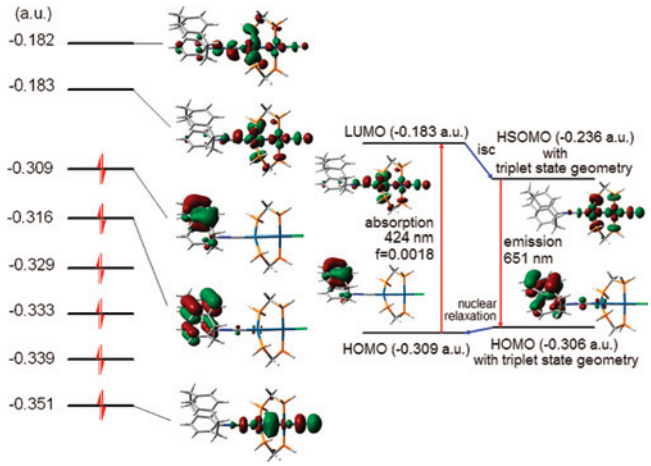

Figure 4. MO energy diagram of the frontier orbitals, MO representations for LUMO + 1, LUMO, HOMO, HOMO − 1, and HOMO − 5, and calculated energetics of the frontier orbitals explaining the lowest-energy absorption and emission of compound **4** using the $[Pt_2(PH_2CH_2PH_2)_2(Cl)(CNPCP)]^+$ model.

Table 4. Computed Singlet−Singlet Transition Energies, Oscillator Strengths, and Their Components for $[Pt_2(PH_2CH_2PH_2)_2(Cl)(CNPCP)]^{+a}$

computed excited states and components (No. MO)			transition energies	oscillator strength
excited state 4:	102 → 106	0.23176	2.9031 eV 427.08 nm	$f = 0.0008$
	102 → 107	−0.14753		
	103 → 106	0.50055		
	103 → 107	−0.31897		
	104 → 106	0.13567		
excited state 5:	105 → 106	0.44435	2.9225 eV 424.23 nm	$f = 0.0018$
	105 → 107	0.53986		
excited state 11:	104 → 106	−0.47011	3.1471 eV 393.96 nm	$f = 0.0749$
	104 → 107	−0.50629		
excited state 18:	99 → 106	−0.11704	3.3878 eV 365.98 nm	$f = 0.0238$
	102 → 107	0.15872		
	103 → 106	0.34841		
	103 → 107	0.54260		

[a] Transitions with $f = 0$ or 0.0001 are removed. MO 105 = HOMO; MO 106 = LUMO. The excited-state numbering refers to the order from the lowest energy to the highest. Since the singlet−triplet transitions are not considered in this analysis, these are not listed. The positive and negative numbers beside the transition represent the relative probability (i.e., weighing).

The lowest energy excited states generated from the HOMO − 1, HOMO, LUMO, and LUMO + 1 are not associated with the dσ−dσ* manifolds. To find the dσ level that would generate these dσ−dσ* excited states, one has to go down to the HOMO − 5. So, the dσ−dσ* singlet excited-state appears to be placed at higher energy. Table 4 provides the computed singlet−singlet absorption transition energies (TDDFT), oscillator strengths (*f*), and their components using the model complex $[Pt_2(PH_2CH_2PH_2)_2(Cl)(CNPCP)]^+$ for which the geometry was optimized (d(Pt−Pt) = 2.705; d(Pt−P) = 2.323 (average); d(Pt−Cl) = 2.442; d(Pt−C) = 2.012; d(N≡C) = 1.178 Å). The lowest computed energy transitions, 424 and 427 nm, correspond fairly well with the observed shoulder at ∼415 nm for **4** in 2MeTHF at 77 K. The electronic transition exhibiting the largest *f* value (0.0018) is the one that contributes the most to the observed intensity. The low value for *f* is consistent with the observed low absorbance of the 415 nm shoulder. This transition exhibits two major contributions of about the same probability (105 → 106 and 105 → 107; HOMO → LUMO and HOMO → LUMO + 1, respectively). Examination of the frontier MOs of Figure 4 indicates that both contributions for this transition are ligand-to-metal-charge-transfer (LMCT), where L is the π-system of the unsubstituted benzene unit in PCP and M is the dσ* of the C≡N−Pt−Pt−Cl fragment. The orthogonal shape of the MOs and the lack of atomic contributions common to both starting and arriving MOs (i.e., poor overlap) make the *f* value predictably small.

The next transition calculated at 394 nm exhibits an *f* value of 0.0749. This is the transition with the largest *f* and must contribute the most in the low-energy region of the spectra for **4**. This transition also exhibits two major contributions of about the same probability (104 → 106 and 104 → 107; i.e. HOMO − 1 → LUMO and HOMO − 1 → LUMO + 1, respectively). Examination of the frontier MOs of Figure 4 also indicates that both contributions for this transition are ligand-to-metal-charge-transfer (LMCT) as well. The difference is the stronger *f* value, which stems from the better MO overlap, notably between the HOMO − 1 and the LUMO + 1 along the benzene−NC frame. The emission spectra of complex **4** exhibit two long-lived broad bands at 77 K in PrCN and in 2-MeTHF glasses at 480 and 630 nm (Figure 5 and Supporting Information Table 5). The excitation spectrum monitored at 630 nm superposes well with the absorption one.

Despite the resemblance of the band maxima and band shape with other d^9−d^9 homo- and heterobimetallic systems containing a terminal isocyanide ligand,[33,34] the band around 630 nm cannot be assigned to an emission arising from a dσ → dσ* excited state (see below). The geometry of the model complex $[Pt_2(PH_2CH_2PH_2)_2(Cl)(CN-PCP)]^+$ was optimized (d(Pt−Pt) = 2.712; d(Pt−P) = 2.320 (average); d(Pt−Cl) = 2.445; d(Pt−C) = 1.988; d(N≡C) = 1.209 Å) in the triplet state and its energy was compared (−0.236 au). The optimized geometry exhibits a lengthening of the Pt−Pt, Pt−Cl, and N≡C bonds, consistent with the antibonding nature of these bonds in the LUMO and LUMO + 1. Moreover, no contribution from the N≡C π-system is noticed in this MO. Upon a radiative process, the geometry in the excited-state does not change and the molecule finds itself with a ground-state electronic configuration (i.e., diamagnetic) with a triplet state geometry. For the sake of accuracy in estimating the emission transition energy, the MO diagram of the model compound $[Pt_2(PH_2CH_2PH_2)_2(Cl)(CN-PCP)]^+$ is computed in its triplet state geometry and in its ground-state electronic configuration. The calculated HOMO energy for the level (in its ground-state electronic configuration with its triplet state geometry) is −0.306 au. The shape of the MO is now composed of a π-system distributed on both benzene rings of the PCP unit, resembling that of the HOMO − 1 in Figure 4. The small difference between this value (−0.306 au) and the value for the ground-state geometry (−0.309 au) is consistent with the relatively small calculated excited-state distortion. Taking into account the energetics as summarized in Figure 4, the computed transition energy

(34) Clément, S.; Mohammed Aly, S.; Bellows, D.; Bérubé, J.-F.; Fortin, D.; Brisach, F.; Strohmann, C.; Knorr, M.; Guyard, L.; Harvey, P. D. In preparation.

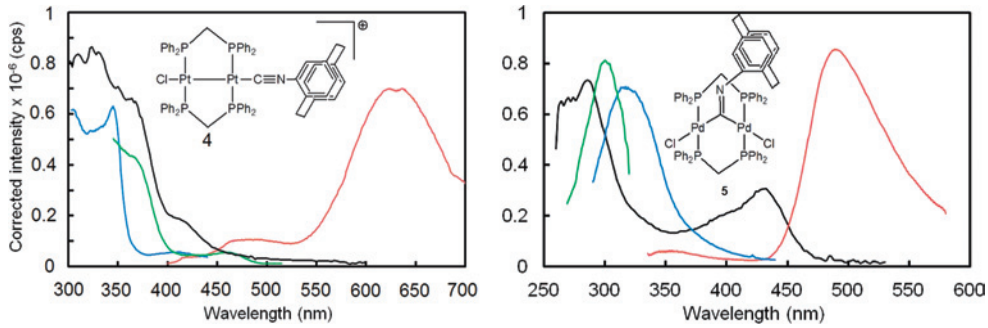

Figure 5. Absorption (black), excitation (blue and green, at 480 and 630 nm for **4** and at 370 and 480 nm for **5**, respectively) and emission (red, at 350 nm for **4** and at 310 nm for **5**) spectra of **4** and **5** in PrCN at 77 K. For 2-MeTHF, see the Supporting Information.

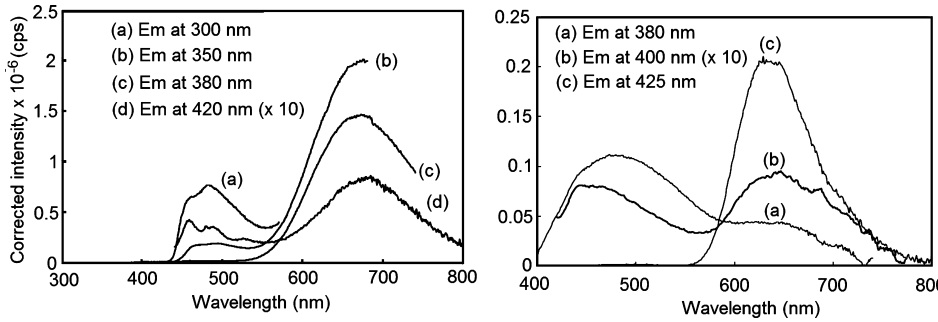

Figure 6. Evolution of the emission spectra of **4** (left) in 2-MeTHF and (right) in the solid state at 77 K with the wavelength of excitation.

for the emission is 651 nm, which corresponds reasonably to the experimental value of the emission maximum (~640 nm). This emission is assigned to the radiative relaxation of the ^{3}LMCT* state. The second emission at 480 nm for complex **4** corresponds to the intraligand (IL) $\pi\pi^*$ phosphorescence of the CN−PCP unit by comparing with the ligand itself. A study of the emission spectra versus the excitation wavelength (Figure 6) shows that the relative ratio of the two emission bands is a function of the selected wavelength. This result indicates that the relaxation of the upper excited states (i.e., $^{1,3}\pi\pi^*$) to the lower excited levels does not necessarily pass through the same deactivation pathway despite structural connectivity. The excitation spectra for the 640 and 380 nm emissions are different (Figure 5). The excitation spectrum for the (IL) $\pi\pi^*$ phosphorescence exhibits a maximum that is blue-shifted with respect to the absorption bands. The band maximum is consistent with the nature of the ligand absorbing in the blue region.

The excitation spectrum of the LMCT emission follows a trace that is red-shifted, corresponding reasonably to the absorption band in the low-energy region. This observation suggests that the electronic communication through the C≡N bridge is not perfectly efficient.

The phosphorescence lifetimes (τ_P) for this IL triplet state (~ 0.21 (2-MeTHF) and 0.15 ms (PrCN)) are shorter than that found for **3** (~3.8 and 3.4, respectively), which is consistent with the presence of the heavy metal. The IL fluorescence is absent or too weak to be observed, which is also a consequence of the same heavy atom effect. Compound **4** is also luminescent in the solid state, exhibiting an unstructured broad band at 630 nm (Supporting Information). Notably, the excitation of complex **4** at different wavelengths induces changes in the emission spectra (Figure 6). The relative intensity of the two emission bands could be controlled in this manner, hence opening the door to emission covering the whole visible spectrum (i.e., 400−800 nm).

Table 5. Photophysical Data for Homobimetallic Systems **4** and **5** at 77K

compound **4**[a]	2-MeTHF	PrCN	solid
λ_P (IL $\pi\pi^*$) (nm)	480	480	
τ_P (IL $\pi\pi^*$) (ms)	0.212 ± 0.002	0.145 ± 0.007	
ϕ_P(IL $\pi\pi^*$)	not measured	0.0009 (±10%)	
λ_e(CT) (nm)	630	630	630
τ_e(CT) (μs)	8.85 ± 0.71	9.34 ± 0.03	not measured
ϕ_e(CT)	not measured	0.027 (±10%)	not measured

compound **5**	2-MeTHF	PrCN	solid [b]
λ_F (IL $\pi\pi^*$) (nm)	360	360	
τ_F (IL $\pi\pi^*$) (ns)	0.168 ± 0.034	0.204 ± 0.056	
ϕ_F[b]		0.0009	
λ_P (IL $\pi\pi^*$) (nm)	480	480	
τ_P (IL $\pi\pi^*$) (μs)	0.630 ± 0.001	0.714 ± 0.001	
ϕ_P (IL $\pi\pi^*$)	not measured	0.006 (±10%)	

[a] IL $\pi\pi^*$ refers to the intraligand $\pi\pi^*$ emission. CT refers to the charger transfer emission in **4**. [b] No luminescence was found for **5** in the solid state.

The UV−visible absorption spectra of **5** in PrCN and 2-MeTHF (Figure 4 and Supporting Information Table 4) exhibit short wavelength bands below 320 nm attributed to the PCP residue as well as a broad band at 445 nm. This latter datum compares favorably with those obtained for other dinuclear complexes containing bridging isocyanides.[34] Table 5 lists the photophysical data for **4** and **5**. Contrary to other d^8-d^8 homo- and heterobimetallics systems,[34] the emission spectra of **5** in 2-MeTHF exhibit a strong broad emission centered at 480 nm and a weak luminescence at ~360 nm (Figure 5 and Table 5), which are assigned to the phosphorescence and fluorescence of the PCP−NC unit. No emission is detected in the 550−850 nm region. In an attempt to find a weak emission associated to the presence of the A-frame $Pd_2(dppm)_2X_2(\mu$-L) unit, time-resolved spectroscopy was

used to discriminate this luminescence based on the fact that emission lifetimes are almost always different from one another. This experiment was performed for both complexes **4** and **5** in PrCN at 77 K (see the Supporting Information), but without success. Although the two emission bands at 510 nm (IL $\pi\pi^*$) and 640 nm (CT) are noted for **4**, only one emission band at 490 nm (IL $\pi\pi^*$) for **5** is observed. The intraligand fluorescence band at 360 nm is also observed in PrCN at 77 K.

According to Kasha's rule,[35] the upper excited states should deactivate to the lowest excited-state prior to observing emission. However, the spectra exhibit clear evidence of luminescence arising from upper excited states.

These upper energy emissions are observable due to the lack of efficient nonradiative relaxation (i.e., communication) between the upper states localized in the PCP ligand (IL $\pi\pi^*$) and the lowest energy excited states located in the A-frame $Pd_2(dppm)_2X_2(\mu\text{-L})$ complex (the nature of the HOMO and LUMO is presented below). Among the nonradiative processes, energy transfer from an excited donor (PCP) to an acceptor (A-frame $Pd_2(dppm)_2X_2(\mu\text{-L})$) is also a possibility to consider, conjugated or not, since through-bond and through-space energy transfer processes exist. Knowing that the triplet energy transfers are generally slow,[35,36] it is likely that the "localized" radiative relaxation processes (i.e., phosphorescence from the IL $\pi\pi^*$) are more efficient, rendering it observable. All in all, despite conjugation through the C≡N group, the electronic communication across this bridge appears modest for **4** and **5**. Knowing that the triplet energy transfer operates via a Dexter mechanism (i.e., double electron exchange),[37] a single electron transfer across the C≡N bridge appears unlikely. This conclusion is consistent with the fact that isocyanide coordination polymers are relatively rarely reported to be conducting (where conductivity proceeds across the conjugated CN group).[38,39]

In support for the assignment for the two observed emissions arising from intraligand $\pi\pi^*$ of PCP, the excitation spectrum of **5** is analyzed. There is a clear mismatch between the excitation and absorption spectra where the lowest energy absorption signal between 375 and 475 is absent from the excitation spectra. Instead, the excitation spectra exhibit a maximum in the 300 nm region, exactly where the PCP−NC ligand (compound **3**) exhibits its maximum in the absorption spectra. Emission from this state is broad and featureless as in **5**. No luminescence was observed in the solid state or at room temperature for **5**. The MO description for compound **5** is addressed the same way as for **3** and **4**, using the model compound $[Pd_2(\mu\text{-}PH_2CH_2PH_2)_2(Cl)_2(\mu\text{-CN−PCP})]$. The MO energy diagram (Figure 7) exhibits the HOMO (−0.196) and LUMO (−0.083 au) along with other frontier orbitals. These MOs are composed of Pd $d_{x^2-y^2}$, P p_y, and Cl p_x, forming M−L antibonding σ-interactions. Moreover, the HOMO exhibits an in-plane atomic contribution from the p_x lone-pairs of the bridging C-atom forming Pd−C π-bonding interactions, whereas the LUMO shows a weak lone pair C σ^* contribution forming symmetric antibonding σ^*−Pd-C interactions.

The lowest energy absorption band spreading from 375 to 475 nm (Figure 7) is interpreted with TDDFT. The computed three lowest energy singlet excited states are listed in Table 6 and exhibit three different oscillator strengths,

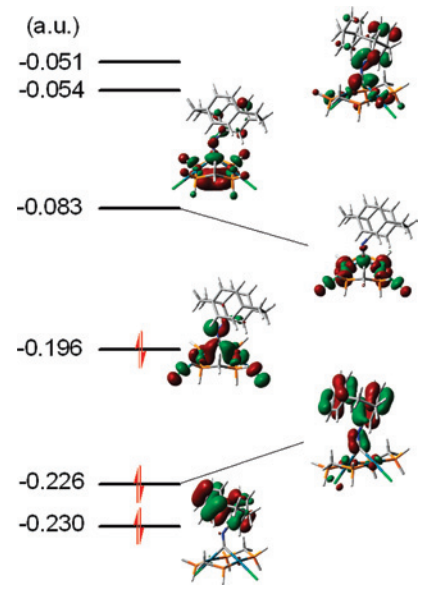

Figure 7. MO energy diagram of the frontier MOs and MO representations for LUMO + 2, LUMO + 1, LUMO, HOMO, HOMO − 1, and HOMO − 2 for $[Pd_2(PH_2CH_2PH_2)_2(Cl)_2(\mu\text{-CN−PCP})]$ model compound.

Table 6. Computed Singlet−Singlet Transition Energies, Oscillator Strengths, and Their Components for $[Pt_2(PH_2CH_2PH_2)_2(Cl)_2(\mu\text{-CN−PCP})]^{+a}$

computed excited states and components (#MO)		transition energies	oscillator strength
excited state 1:	101 → 110 −0.15746	2.6284 eV 471.71 nm	$f = 0.1272$
	109 → 110 0.57275		
	109 → 111 −0.15133		
excited state 2:	109 → 110 0.10920	3.0247 eV 409.90 nm	$f = 0.0151$
	109 → 111 0.65086		
	109 → 112 −0.18729		
excited state 3:	106 → 110 0.44513	3.0871 eV 401.63 nm	$f = 0.0161$
	107 → 110 0.12625		
	108 → 110 0.41156		
	109 → 110 −0.13404		
	109 → 112 −0.18543		

[a] MO 109 = HOMO; MO 110 = LUMO. The excited-state numbering refers to the order from the lowest energy to the highest. The positive and negative numbers beside the transition represent the relative probability (i.e., weighing).

(35) Turro, N. J. *Modern Molecular Photochemistry*; University Science Books: Sausalito, CA, 1991.
(36) Lakowicz, J. R., *Principles of Fluorescence Spectroscopy*, Springer, New York, 2004.
(37) Harvey, P. D. In *The Porphyrin Handbook II*; Kadish, K. M., Smith, K. M., Guilard, R., Eds.; Academic Press: San Diego, 2003; Vol. *18*, pp 63−250.
(38) (a) Jaffe, I. *Rev. Inorg. Chem.* **1993**, *13*, 76. (b) Carson, C. G.; Gerhardt, R. A.; Tannenbaum, R. J. *Phys. Chem. B* **2007**, *111*, 14114–14120. (c) Carson, C. G.; Gerhardt, R. A.; Tannenbaum, R. *PMSE Preprints* **2007**, *96*, 238–239. (d) Tannenbaum, R. *Chem. Mater.* **1994**, *6*, 550–555. (e) Carson, G. C.; Gerhardt, R. A.; Tannenbaum, R. *J. Phys. Chem. B* **2007**, *111*, 14114–14120. (f) Yu, M. P. Y.; Yam, V. W.-W.; Cheung, K.-K.; Mayr, A. *J. Organomet. Chem.* **2006**, *691*, 4514–4531. (g) Ryu, H.; Kang, Y.-G.; Knecht, S.; Subramanian, L. R.; Hanack, M. *Syn. Met.* **1997**, *87*, 69–73.
(39) The ethynyl linker (−C≡C−) provides polymers of better conjugation. Recent papers by our group show clear evidence for conjugation and good communication across the polymer backbone. See: Gagnon, K.; Mohammed Aly, S.; Brisach-Wittmeyer, A.; Bellows, D.; Berube, J.-F.; Caron, L.; Abd-El-Aziz, A. S.; Fortin, D.; Harvey, P. D. *Organometallics* **2008**, *27*, 2201–2214, for example.

where the largest one is distinctive by 1 order of magnitude (excited state 1). The predicted position (471 nm) falls where it is anticipated based on the experimental spectrum. The major component of this excited-state arises from the HOMO → LUMO excitation. This excitation resembles that of a d−d transition. The observed fluorescence and phosphorescence in **5**, assigned at first glance to intraligand $\pi\pi^*$ emissions, are indeed appropriately assigned, except that a comment must be made. In Figure 7, the ligand-localized π-manifolds are found as the HOMO − 1 and HOMO − 2 at energies similar to that presented for **3** (Figure 2). However, the two corresponding PCP localized antibonding analogues are found as LUMO + 2 (−0.051) and LUMO + 4 (−0.021 au; not shown), except that a contribution of the $Pd_2(dppm)_2(Cl)_2(\mu\text{-L})$ unit is computed because of appropriate symmetry.

Conclusion

Two homobimetallic complexes **4** and **5** bearing PCP-NC as a building block were prepared, and their photophysical properties investigated. The isocyanide bonding mode (bridging vs terminal) depends on M, leading to the Pt−Pt-bonded monocationic [ClPt(μ-dppm)$_2$Pt(CN−PCP)]Cl (**4**) or to the A-frame [ClPd(μ-dppm)$_2$(μ-C═N−PCP)PdCl] (**5**) complexes, respectively. These two isocyanide-containing complexes in frozen glasses at 77 K exhibit a weak fluorescence (for **5**) and a phosphorescence (for **4** and **5**) arising from the PCP unit (mainly IL $\pi\pi^*$ with some charge transfer character). Both luminescence bands are placed at higher energy above the charge transfer one (arising from the IL $\pi\pi^*$ PCP → dσ^* $Pt_2(dppm)_2Cl$), indicating that the nonradiative relaxations from the these upper states to the lowest one are not efficient. This observation clearly indicates that the conjugated C≡N linker has modest electronic communication properties. Moreover, upon excitation at different wavelengths, the relative intensity of the two emission bands for **4** is controllable, hence allowing tuning. Hence, these materials built upon a PCP skeleton may be potential candidates for the design of novel photonic devices.

Acknowledgment. P.D.H. and A.S.A. thanks the Natural Sciences and Engineering Research Council of Canada (NSERC) for funding. M.K. thanks the French Ministère de la Recherche et Technologie for financial support and a Ph.D. grant for S.C. as well as the Fonds Québécois de la Recherche en Science Naturelles et en Technologie (FQRNT) for a postdoctoral fellowship for S.C.

Supporting Information Available: ^{1}H and ^{31}P{^{1}H} NMR spectra for complexes **4** and **5**. Time-resolved emission spectra of **3** in PrCN at 77 K. Absorption, excitation and emission spectra of **3** in 2-MeTHF and in the solid state at 77 K. Absorption, excitation, and emission spectra of **4** and **5** in 2-MeTHF at 77 K. Emission spectra in the solid sate for **4**. Selected bond distances and angles for [(^{t}Bu-NC)Pt(μ-dppm)$_2$Pt(NC-*t*Bu)](BF$_4$)$_2$ (crystallographic and optimized geometry data). This material is available free of charge via the Internet at http://pub.acs.org

IC800811J